Intermittency in the Solar Wind Turbulence and the Haar Wavelet Transform

A. Mangeney
Observatoire de Paris-Meudon - email: mangeney@despace.obspm.fr
C. Salem
Space Sciences Laboratory - email: salem@ssl.Berkeley.edu
P.L. Veltri
Universitá della Calabria - email: VELTRI@fermi.fis.unical.it
B. Cecconi
Observatoire de Paris-Meudon - email:baptiste.cecconi@obspm.fr

Abstract

The solar wind is a collisionless, strongly turbulent plasma in supersonic, spherical expansion. In the Alfvenic regime -time scales ranging from a few hours to a tenth of a second- the MHD turbulence exhibit what appears like an inertial domain, with power law spectra, scale invariance and strong intermittency with a mixture of of random fluctuations and small scale "singular" structures as in ordinary fluid turbulence. These singular stuctures take the form of current sheets -as in numerical simulations of MHD turbulence- of shock waves, flux tubes and magnetic holes. I will discuss in particular the use of the Haar Wavelet Transform to analyse the intermittent structure of solar wind turbulence.

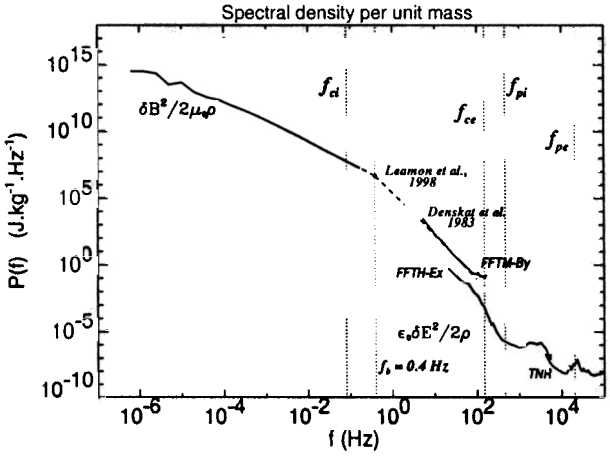

Figure 1: Overview of the magnetic and electric spectral densities

1 Introduction

In the solar wind, the electromagnetic fields and plasma properties show fluctuations over a wide range of time scales with properties which been reviewed in a number of papers (see for example Mangeney *et al*,1991, Goldstein *et al.*,1995, Tu and Marsch, 1995, Horbury, 1999). We do not want here to provide another review paper, but more modestly to point out the advantages of the wavelet transform in the analysis of the intermittence of the solar wind turbulence.

Before discussing this point, it is however useful to describe, even summarily, some of the most basic fetures of solar wind turbulence.

Figure 1 which summarizes some typical observations, taken during 38 days (20th May to 26th June 1995) in the ecliptique plane at the L1 Lagrange point by the Wind spacecraft in a very broad domain of time scales going from the rotation period of the sun to the local electron plasma period. Data from several instruments have been combined. In the low frequency domain, the magnetic field data (with 3 sec resolution) come from the MFI experiment (Lepping *et al.*, 1995) while the plasma data (also with 3 sec resolution) come from the 3D-Plasma experiment (Lin *et al.*, 1995). At higher frequency we have indicated the data obtained by Leamon *et al.* (1998) with the high resolution magnetic field data from the MFI instrument. At still higher frequency, data obtained on board of the Helios spacecraft by Denskat *et al.* (1983) are also reported, as well as data obtained from the FFTM spectral analyzer from the Waves experiment (Bougeret *et al.* , 1995). All these data concerned the magnetic field measurements which are available up to few hundred Hertz where the instrumental noise becomes usually dominant; above a few tens of Hertz, ac elctric field data from the FFTH and TNR spectral analyzers from the Waves experiment (Bougeret *et al.* , 1995) have been also plotted. Note that since, as usual, the ob-

Proceedings of the Les Woolliscroft Memorial Conference / Sheffield Space Plasma Meeting: Multipoint Measurements versus Theory, Sheffield, United Kingdom, 24 — 26 April 2001 (ESA SP-492, July 2001)

servations are made at a given point - the spacecraft - which moves very slowly compared to the speed V_{SW} of the solar wind, a temporal variation on a period t corresponds to a spatial variation on a scale $l = tV_{SW}$ along the direction of the flow, i.e. the radial direction if the fluctuations are "frozen" in the solar wind. This is a good approximation since V_{SW} is much larger that the characteristic speeds of the solar wind plasma, either the Alfven speed v_A or the ion sound speed c_s.

In the figure 1, spectral power density per unit masses are plotted against frequency because these quantities are relatively insensitive to variations with radial distance, allowing easy comparison with data obtained in other regions of the solar wind. At the largest scales, i.e. the longest periods, the kinetic energy dominates - corresponding to the differential streaming of fast and slow winds. In the "Alfvenic" range, the domain of frequencies between $f_* \sim (10\ hours)^{-1}$ and the proton gyrofrequency $f_{ci} = \Omega_i/2\pi$ which is on the average ~ 0.1 Hz during the period considered here, ($\Omega_i = eB/M$, B being the magnitude of the magnetic field and $e$and M the charge and mass of a proton), there is is roughly equipartition between magnetic and kinetic energy. Around the proton cyclotron period, the magnetic power spectrum begins to steepen. It is surprising to see how well data coming from different instruments, taken at different times, do match together (note however that the FFTM data are contaminated by noise around 100Hz). At still higher frequencies, between the proton and electron plasma frequencies $f_{pi} = \omega_{pi}/2\pi \sim 500$ Hz and $f_{pe} = \omega_{pe}/2\pi \sim 20$ kHz ($\omega_{pi} = (ne^2/\mu_0 M)^{1/2}$, $\omega_{pe} = (ne^2/\mu_0 m)^{1/2}$, n the plasma number density, m the electron mass and μ_0 the magnetic permeability of vacuum) one observes the "ion accoustic noise", a highly intermittent electrostatic noise which rises several order of magnitude above the thermal noise of the plasma.

The spectral densities shown in figure 1 are averaged over the whole 38 days period considered here; this means in particular that we have included the succession of fast and slow streams observed during this period in the low frequency part of the spectra and that we have not taken into account the differences in the Alfvenic range between these fast and slow streams.

The "Alfvenic" range has been extensiveley studied, to answer the question of wether what we observe in this range is the result of a NL cascade or the remains of a spectrum of Alfven waves injected in the corona into the expanding Solar Wind. There is now a general consensus that, within the inner heliosphere, at least the small wavelengths are affected by non-linearities and that, correspondingly, energy cascades towards smaller and smaller wavelengthes. While the Alfvenic turbulence is observed to be made of finite amplitude Alfven wave type fluctuations propagating away from the sun, the nonlinear cascade does not seem to be strongly affected by the *Alfven* effect which will be described below, contrary to the prediction by Iroshnikov (1963), Kraichnan (1965) and Dobrowolny *et al.* (1980). Indeed, one of the important characteristics of the turbulence in the range $f_* \leq f \leq f_{ci}$ is that the power spectra have the form of power laws with spectral indices varying the from the Kolmogorov K41 prediction of $-5/3$ - for the magnetic field fluctuations to the IK prediction of $-3/2$ for the velocity fluctuations (Goldstein *et al.*,1995, Tu and Marsch, 1995, Horbury, 1999).

The privileged tool in the analysis of turbulence in space plasmas has long been the windowed Fourier transform (WFT) where the piece of signal contained in a time window of length T is analyzed to determine how each frequency band contribute to the total variance of that particular piece of signal. The window is then moved in order to cover the whole interval under consideration, and get an idea about the time variation of this spectral information. The WFT has therefore a time resolution equal to T and a frequency resolution $\Delta f = 1/T$, so that if one decreases the window length to have better time resolution, one deteriorates the frequency resolution. Actually the WFT is one particular member of a family of tools of signal analysis depending on two parameters - the first one being the shift between successive positions of the analyzing window and the second one characterizing the resolving efficiency at a given position of the window. Another class of that family is the wavelet transform, which favors the time resolution at the expense of frequency resolution, in degrees depending on the particular wavelet which is used. For example, the Haar wavelet, used here, has a very good time resolution, but a poor frequency resolution. While the use of this wavelet is not convenient in situations where narrow spectral peaks are the objects of the investigation, it seems to be well suited to the study of solar wind turbulence, characterized by featureless average power spectra, and strongly intermittent behaviour, similar to what is observed in strongly turbulent neutral flows, where the fluid velocity components measured at a given point look like a usual random signal but with intermittent bursts of strong variations (see for example Sreenivasan and Antonia, 1997).

Because the wavelet trandform remains relatively unfamiliar in the space physics community, we shall present now a very simple description of the Haar wavelet transform (HWT), refering the reader for further details, for example to the book *Wavelet in Geophysics*, (*Wavelets Analysis and its Applications, Vol 4*).

2 The Haar wavelet transform

Consider $N = 2^M$ successive samples $\{y_j\}_{1 \leq j \leq N}$ measured at times $t_j = (j-1)\Delta t$ of a centered random quantity y, with variance σ_y^2. The discrete orthogo-

nal wavelet transform (see for example, Katul *et al.*, 1994) $a_y(i,m)$ of the signal is defined as the discrete convolution product of y with a scaled and translated "analysing " wavelet $\psi(t)$:

$$a_y(i,m) = 2^{-m/2} \sum_{l=0}^{N} \psi(\frac{t_l - t_{i,m}}{\Delta t_m})\, y_l \qquad (1)$$

At "scale" $m \leq M$, the scale factor is $\Delta t_m = 2^m \Delta t$ while the wavelet coefficient a_y is sampled at times $t_{i,m}$ $= i\Delta t_m$.

There is a similarity with the WFT which can be summarized as follows. In the WFT, one chooses a window of analysis, say $T = 2K\Delta t$, $K < N/2$, to achieve a given frequency resolution $\Delta f = 1/T$ and this window is diisplaced with steps equal to T. At each successive position of the window $t_k^{(K)} = (k - 1/2)T$, $k = 1, ...,$ one performs a discrete Fourier transform

$$b_K(f_l, k) = \frac{1}{2K} \sum_{j=k-K}^{k+K} y_j \exp 2\pi i l t_j / T \qquad (2)$$

giving $K + 1$ complex amplitudes at frequencies i f_l $= l\Delta f$, $l = 0, ..., K$ for each position of the window. Equation (2) can be written in a form similar to equation (1)

$$b_K(f_l, k) = \sum_{l=0}^{N} \psi_{wft}\left(l\left(t_j - t_k^{(K)}\right)\right) y_j$$

with

$$\psi_{wft}(t) = \left(\frac{1}{2K}\right) Y_T(t) \exp\left[2\pi i \frac{t}{T}\right]$$

$Y_T(t)$ being the characteristic function of the interval $-T/2 \leq t \leq T/2$. However, there is a basic difference since only the exponential part of the analysing signal is scaled and translated, the window remaining of constant support.

For the WFT, the Bessel-Parseval theorem ensures that the total variance$< y^2 >_T$is the sum of the spectral densities $P(f_l) = \|b_K(f_l)\|^2 T$ in each K independant frequency bands

$$\sigma_y^2 = \frac{1}{2K} \sum_{j=k-K}^{k+K} (y_j)^2 = \sum_{l=1,K} P(f_l)\, \Delta f \qquad (3)$$

Similarly the $N - 1$ wavelet coefficients $\{a_y(i,m)\}$, for $i = 1, .., 2^{M-m}$and $m = 1, .., M$ satisfy a Bessel-Parseval identity

$$N\sigma_y^2 = \sum_{m=1}^{M} \sum_{i=1}^{2^{M-m}} |a_y(i,m)|^2 \qquad (4)$$

and are fully equivalent to the data

In writing equation 2, we have assumed a square window for simplicity; other windows can be used to reduce noise, sidelobe effects, et.... The important point here, however, is that each Fourier component can be viewed as a mean value over the same $2K$ points, so that all coefficients have the same time resolution T what is clearly unsatisfactory if the signal presents localized spikes of duration smaller than T superposed on more regular variations covering the whole range of available frequencies.

Therefore, it seems convenient to use a wavelet transform (HWT), because of its good time resolution, which allows to localise singular features in the distribution of these fluctuations.

The particular wavelet we shall use here is the Haar wavelet defined as

$$\begin{aligned} \psi(t) &= 1 \ for\ 0 < t < 1/2 \\ &= -1 \ for\ 1/2 < t < 1 \\ &= 0 \ elsewhere \end{aligned}$$

In that case, to obtain the wavelet coefficients at scale $m + 1$ we evaluate first the smoothed (over 2^m points) signal $y^{(m)}$ made up of the 2^{M-m} samples

$$y_i^{(m)} = 2^{-m} \sum_{l=i-2^m}^{l=i+2^m} y_l$$

calculated at the points

$$t_i^{(m)} = (2m-1)\,\Delta t/2 + (i-1)\Delta t_m, i \quad \leq i \leq 2^{M-m}$$

separated by the scaled time interval Δt_m. The successive smoothing on larger and larger scales can be obtained by the simple iteration:

$$y_i^{(m+1)} = \frac{1}{2}\left\{y_{2i+1}^{(m)} + y_{2i}^{(m)}\right\}$$

($m = 0$ correspond to the original data) while the "fluctuation" $\delta y_i^{(m+1)}$ at that scale $m + 1$ is given by

$$\delta y_i^{(m+1)} = \frac{1}{2}\left\{y_{2i+1}^{(m)} - y_{2i}^{(m)}\right\}$$

and is related to the discrete wavelet coefficient by

$$a_y(i, m+1) = 2^{m/2} \delta y_i^{(m+1)}$$

as may be very easily checked.

The upper panel of figure 2 illustrates this procedure for the calculation of the $i = 21$ wavelet coefficient at scale $m = 5$ of the x component B_x of the magnetic field, $a_{Bx}(21, 5)$. The initial data, a small arbitrary sample of data from the Cluster FGM experiment at 4 sec resolution, are plotted in the upper panel for the time interval [4.3-4.4] UT versus time in decimal hours;

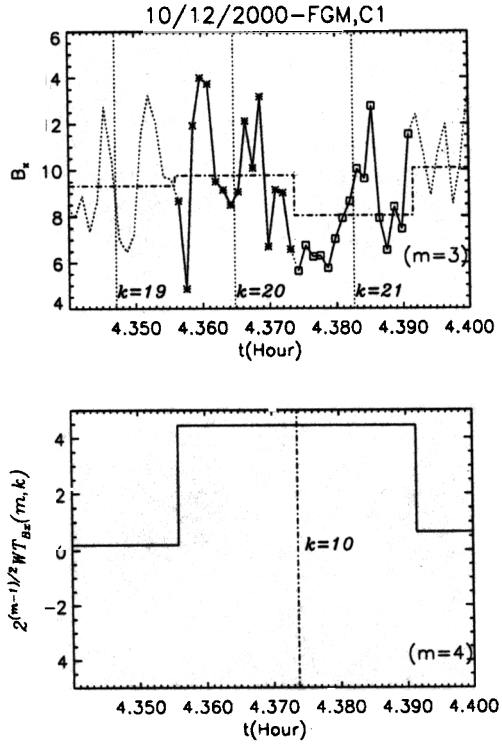

Figure 2: Illustration of the computation of wavelets coefficients

in this case, $t_i^{(m)} = 4.35647$ and $\Delta t_m = 0.0172262$ so that the corresponding wavelet after scaling and translation is defined by $\psi_{k,m}(t) = 1$ for $0 < t_c - t < 0.0172262$, $\psi_{k,m}(t) = -1$ for $0 < t - t_c < 0.01722621$ and $\psi_{k,m}(t) = 0$, elsewhere.

In the same panel of figure 2 , we have also drawn this wavelet or more precisely the function $(bx1 + bx2)/2 + (bx1 - bx2)\psi_{k,m}(t)/2$ where $bx1$ and $bx2$ are respectively the mean values of the signal in the intervals corresponding to the positive and negative parts of the wavelet, indicated by the stars and squares on the B_x plot; they are also, up to scaling factors, the values of $y^{(m)}(11)$ and $y^{(m)}(12)$. In the lower panel of the figure 2 we displayed the corresponding wavelet coefficients, more precisely the fluctuations $\delta y^{(m+1)}$.

The wavelet coefficients are still random quantities whose statistical properties allow to characterize the state and the degree of "smoothness" of the turbulent field. Consider for example the case when y is a white, gausian random noise. Such a random function is nowhere differentiable (even in a statistical sense, known under the name of mean square differentiability); indeed there is mean square differentiability only if high frequencies are not too prevalent i.e if $\int df\, f^2 P(f) < \infty$; then mean square derivative and ordinary derivative are almost everywhere identical (see Doob,1953). For a white noise, on the contrary,

$$\lim_{\tau \to O} \frac{|y(t+\tau) - y(t)|}{\tau} \to \infty$$

even in a statistical sense, since $\left\langle |y(t+\tau) - y(t)|^2 \right\rangle = 2\sigma_y^2 = constant$, independant of τ. In the discrete case, the rms value of the derivative is of course limited to $\sqrt{2}\sigma\ /\Delta t$.

One can wonder wether smoothing the signal over an interval T, for example by introducing

$$\overline{y} = \frac{1}{T}\int_{-T/2}^{T/2} dt' y(t+t')$$

results in better differentiability. Using T to measure the displacement $\tau = \zeta T$, the "derivative at scale T " can be defined as

$$D^T y = \lim_{\zeta \to O} \frac{|\overline{y}(t+\zeta T) - \overline{y}(t)|}{\zeta T} \propto \frac{1}{\zeta}$$

which diverges also for $\zeta \to O$ since the variance of $\overline{y}$ is σ_y^2/T

In terms of the wavelet coefficients of the signal y and its successive smoothings $y^{(m)}$, the "derivative at scale m" can be also defined as

$$Dy^{(m)} = 2\frac{\delta y_i^{(m+1)}}{\Delta t_m} = 2^{-3m/2}\left(\frac{2a_y(i,m+1)}{\Delta t}\right)$$

which is a random variable with a rms value $\left[Dy^{(m)}\right]_{rms} = 2^{-3m/2}\left[Dy^{(0)}\right]_{rms}$, where $\left[Dy^{(0)}\right]_{rms} = 2\sigma_y/\Delta t$ is the smallest scale derivative for our gaussian example. This relation is more illustrating when proceeding from large to small scales

$$\left[Dy^{(m)}\right]_{rms} = 2^{3(M-m)/2}\left[Dy^{(M)}\right]_{rms} \sim (\Delta t_m)^{-3/2}$$

which shows that $y^{(m)}$ has a statistically greater and greater derivative as the scale decreases, $m \to O$, $\Delta t_m \to \Delta t$ a consequence of the well known fact that a gaussian noise is not differentiable.

For a gaussian noise, the statistics of the variable $Dy^{(m)}$ is fully determined by by its variance, $\left[Dy^{(m)}\right]_{rms}^2$. If the noise is not gaussian, the second order moment $\left[Dy^{(m)}\right]_{rms}^2 =< \left(Dy^{(m)}\right)^2 >$ is not sufficient to determine its statitical properties; the most complete information is provided by the probability distribution function (pdf) of $Dy^{(m)}$ or, equivalently the full set of moments $< \left(Dy^{(m)}\right)^{2p} >$, $p = 1, 2, ...$ These moments are determined by the "structure functions" $S_y^p(t,m) =< \left|y^{(m)}(t+\Delta t_m) - y^{(m)}(t)\right|^{2p} >$ of the smoothed signal $y^{(m)}$ and consequently by the moments of the wavelet coefficients $< |a_y(i,m)|^{2p} >$

$$S_y^p(t,m) \sim \frac{< |a_y(i,m)|^{2p} >}{\left(2^{m/2}\Delta t\right)^{2p}} \qquad (5)$$

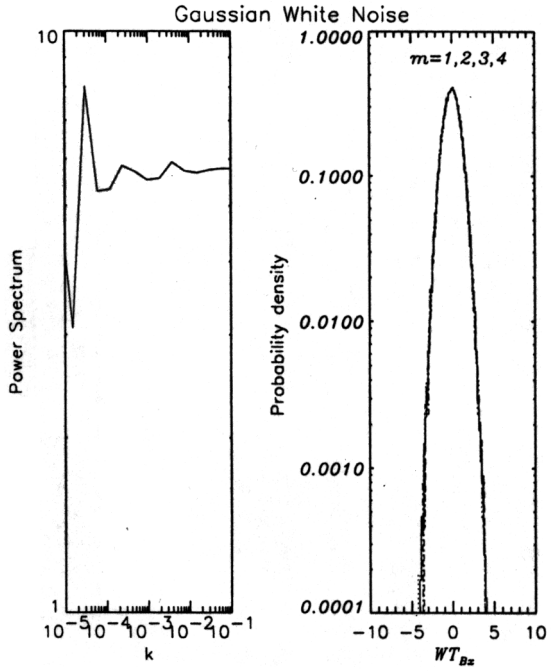

Figure 3: Wavelet spectral density and probability distribution of wavelet amplitudesi for a gaussian signal

Note that the definition (5) of the structure function refers only to quantities defined at scale m while the conventional definition of the structure function at scale m which would be $< |y(t+\Delta t_m) - y(t)|^{2p} >$ contains still informations about scales which are finer that m; in practice this difference does not appear to be important. By comparing the relations (3) and (4) it can be seen that the second order moment ($p = 1$) at scale m is directly related to the usual power spectral density (see Katul *et al.*, 1994) at frequency $f_m = 1/\Delta t_m$:

$$P_y(f_m) = \frac{< |a_y(m)|^2 > \Delta t}{\ln(2)} \qquad (6)$$

Note that the average is taken over the interval corresponding to the WFT window and that $P_y(f_m)$ is actually also an average of the WFT power spectrum over logarithmically spaced frequency bands $\Delta f_m = \ln(2)/\Delta t_m$, what explains why power spectral density calculated in this way are much smoother than those obtained directly from WFT.

The wavelet spectrum is plotted in the left panel of figure 3 while the histograms of the wavelet coeeficients for $m \leq M$ are plotted in the right panel with a different symbol for each value of m. It is seen that the histograms are gaussian and almost identical to the probabilty law of the random variable y. This is easily understood since the mean values $y^{(m)}$ are also distributed in a gaussian way but with an *rms* valueof $y^{(m)}_{rms} = 2^{-m/2} y_{rms}$ implying that the fluctuation $\delta y^{(m+1)}$ is gaussian with the same *rms* value. With the proper scaling then, $\left[a_y^{m+1}\right]_{rms} = 2^{m/2}\left(2^{-m/2} y_{rms}\right) = y_{rms}$ as observed in figure 3.

Let us now consider a more sophisticated signal, introduced by Benzi *et al.* (1993)), which has the property that

$$S_y^p(m) \sim m^{\zeta_p}$$

where ζ_p is not a linear function of p as one would expect in a gaussian signal but is very similar to what is observed in developped turbulence. This property defines a multiaffine random variable, a central concept in the mutifractal formalism. The signal is constructed in the following way. First one chooses arbitrarily the value of the unique wavelet coefficient at the coarsest level. At the next level, $m = M - 1$, the two wavelet coefficients $a_y(1, M-1)$ and $a_y(2, M-1)$ are obtained by multiplying a_y^M by random numbers

$$\begin{aligned} a_y(1, M-1) &= \xi_1 \eta_1 a_y^M \\ a_y^M(2, M-1) &= \xi_2 \eta_2 a_y^M \end{aligned} \qquad (7)$$

where the ξ_k are chosen independantly in a random sequence of ± 1 and the η_k are also independant random numbers -the particular choice of the probability law having no influence on the qualitative properties of the model). This procedure is repeated at each level of decreasing m with the same rule relating the mother wavelet amplitude and its two daughters.

The specific realisation which we have used here is characterized by $M = 17$, $a_y^M = 1.777$ while the η_k are chosen with uniform probability in the interval $[0.31, 0.89]$.

The corresponding wavelet spectrum is plotted in the right panel of figure 4 and the wavelet coeeficients histograms for $m \leq M$ are plotted in the left panel. It is seen that the spectrum has the shape of a power law; while the pdf's $\Pi_m(a_y(m))$ obey the scaling relation

$$2^{-(m-1)/2} \Pi_m(2^{(m-1)/2} a_y(m)) = \Pi_1(a_y(1))$$

which is, as expected different, from the preceding gaussian case, and indicates a self similarity between the statistical behaviour at the various scales. Note that this scaling relation has been used in figure 4 to superpose all pdf's.

3 Phenomenologies

In the absence of a well accepted theory, a number of phenomenological models have been developped in fluid dynamics or MHD to understand the observed intermittency and scaling properties of fully developped turbulence.

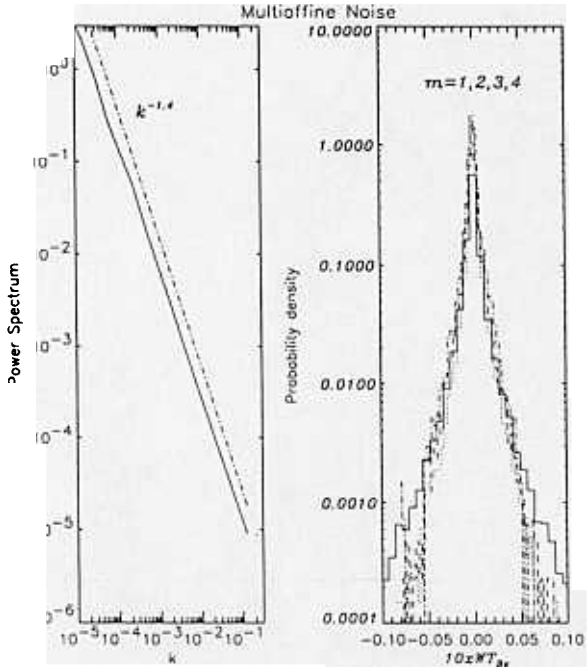

Figure 4: Wavelet spectral density and probability distribution of wavelet amplitudesi for a multiaffine signal

3.1 Incompressible neutral fluid

The simplest case is that of an incompressible fluid, whose governing equations in the limit of infinite Reynolds number $R_e \to \infty$, the Euler equations, are

$$\frac{\partial \mathbf{u}}{\partial t} + \mathbf{u} \cdot \nabla \mathbf{u} = -\nabla p$$

$$\nabla \cdot \mathbf{u} = 0$$

$\mathbf{u}$ being the velocity and p the pressure. It is important to note that these equations are invariant under the scale transformation

$$\mathbf{r} \to \zeta \mathbf{r}; \mathbf{u} \to \zeta^{\mu} \mathbf{u}; t \to \zeta^{1-\mu}; p \to \zeta^{2(\mu-1)} p \quad (8)$$

ζ being an arbitrary scale factor and μ an as yet undetermined exponent. One may assume that these transformations apply also between different scales if some scaling property is observed, ζ being then the ratio between the two scales.

The following argument, due to Kolmogorv (1941, referred to as K41 phenomenology) allows to determine the exponent μ. In an incompressible fluid, an "eddy", that is a perturbation $\delta \mathbf{u}_l$ of scale l (the generalisation of the fluctuation introduced above) will not propagate but will be advected by other eddies of larger scale; if the scale difference is too large the smaller eddy will be advected almost without deformation by the larger ones; significant exchange is expected only in the interaction of eddies of similar sizes which are brought into contact. Since there are no typical time or length scales imposed from the outside, the only typical time which one can think of for such an interaction at scale l is the "turn over" time

$$\tau_{NL} \sim \frac{l}{\delta u_l}$$

During this time the two eddies will exchange an energy of the order of their own energy $(\delta u_l)^2$ so that the energy flux at scale l is

$$\epsilon_l \sim \frac{(\delta u_l)^2}{\tau_{NL}} \sim \frac{(\delta u_l)^3}{l}$$

The scaling properties of the transfer rate ϵ_l under the transformation (8) are

$$\epsilon_l \sim \frac{(\delta u_l)^3}{} \to \zeta^{3\mu-1} \epsilon_l$$

In the inertial range, and in the stationary state, it seems natural to require that the energy flux is independant of the scale and equal to a constant ϵ

$$\epsilon_l = \epsilon$$

This specifies the index μ of the scale transformation, since then $3\mu - 1 = 0$ and $\delta u_l \sim (\epsilon l)^{1/3}$, leading to the well known Kolmogorov power spectrum. Note that the velocity signal, in that case, is not mean square differentiable. Clearly this is valid only in the inertial regime; at smaller scale, dissipative effects become important so that the spectral power drops abruptly and differentiability is recovered.

This model is essentially based on the scaling invariance of the Euler equations and simple phenomenological considerations, without reference to the details of the nonlinear interactions wich are responsible for the energy transfers.

3.2 Incompressible MHD and the Alfven effect

What happens in a magnetized plasma? We assume now that the fluid is electrically conducting and interacts with a magnetic field $\mathbf{B}$ while being still incompressible, so that the mass density $\varrho = \varrho_0 = const$, and as a consequence, the velocity field $\mathbf{v}$ is purely solenoidal, $\nabla \cdot \mathbf{v} = 0$. Then the governing equations can be simplified, by using dimensionless variables. Let L be a characteristic length, U , a characteristic fluid velocity, $t_H = L/U$, a characteristic time, B_0 a characteristic magnetic intensity and $c_A = B_0/(\mu_0 \varrho_0)^{1/2}$ a characteristic Alfven velocity. Using the dimensionless variables

$$\mathbf{r} = L\hat{\mathbf{r}}; \mathbf{t} = t_H \hat{\mathbf{t}}; \hat{\mathbf{u}} = = \frac{\mathbf{v}}{U}; \mathbf{b} = \frac{c_A}{U} \frac{\mathbf{B}}{B_0}; \hat{p} = \frac{p}{\varrho_0 U^2}$$

the basic equations of incompressible MHD can be written as

$$\frac{\partial \mathbf{b}}{\partial t} = \nabla \times (\mathbf{u} \times \mathbf{b}) + \frac{1}{R_m}\Delta \mathbf{b} \tag{9}$$

$$\frac{\partial \mathbf{u}}{\partial t} + \mathbf{u} \cdot \nabla \mathbf{u} = -\nabla p + (\nabla \times \mathbf{b}) \times \mathbf{b} + \frac{1}{R_f}\Delta \mathbf{u} \tag{10}$$

$$\nabla \cdot \mathbf{u} = \nabla \cdot \mathbf{b} = 0$$

These equations contain only two parameters the fluid Reynolds number R_e and the magnetic Reynolds number R_m

$$R_e = \frac{UL}{\nu}; R_m = \frac{UL}{\lambda}$$

which measure the ratio of the dissipative terms to the nonlinear ones. In what follows, we shall consider only the inertial regime where R_e and $R_m \to \infty$.

Equations (9) and (10) can be combined together to form equations for the Elsässer amplitudes $\mathbf{z}^{\pm} = \mathbf{u} \pm \mathbf{b}$ (Elsässer, 1950, 1956)

which can be written as:

$$\frac{\partial \mathbf{z}^{\pm}}{\partial t} + \mathbf{z}^{\mp} \cdot \nabla \mathbf{z}^{\pm} = -\nabla p \tag{11}$$

$$\nabla \cdot \mathbf{z}^{\pm} = 0$$

In these equations the pressure p is not an independant variable; it serves only to maintain the incompressibilty constraint since, usually $\nabla \cdot [\mathbf{z}^{\mp} \cdot \nabla \mathbf{z}^{\pm}] \neq 0$; it is indeed determined by the equation obtained by the divergence of equation (11):

$$\Delta p = -\nabla \cdot [\mathbf{z}^{\mp} \cdot \nabla \mathbf{z}^{\pm}]$$

If there is a uniform magnetic field $\mathbf{b}_0$ of amplitude 1 in these units, and directed, say along the $\mathbf{e}_x$ axis, it is convenient to separate out this component so that the definition of the Elsässer amplitudes is slightly modified, $\mathbf{z}^{\pm} = \mathbf{u} \pm (\mathbf{b} - \mathbf{b}_0)$ and

$$\frac{\partial \mathbf{z}^{\pm}}{\partial t} \pm \frac{\partial}{\partial x}\mathbf{z}^{\pm} + \mathbf{z}^{\mp} \cdot \nabla \mathbf{z}^{\pm} = -\nabla p \tag{12}$$

One important property of equations (12) is that they have finite amplitude Alfven waves as solutions, propagating at the Alfven speed without distortion along the $\mathbf{e}_x$ axis, either towards positive x

$$\mathbf{z}^- = 0, \mathbf{z}^+ = \epsilon f(x-t), \; p = const$$

or towards negative x,

$$\mathbf{z}^+ = 0, \mathbf{z}^- = \epsilon g(x+t), \; p = const$$

where f and g are arbitrary functions fixed by the initial conditions, and ϵ a constant polarisation vector which is arbitrary except that it has to be perpendicular to the ambiant magnetic field $\mathbf{b}_0$.

However, since the equations are not linear, a linear superposition of these two solutions has no chance to be a solution! On the contrary this is the best situation to have significant nonlinear effects, since the two equations (12) clearly show that the nonlinear terms are proportional to the amplitudes of the two waves propagating in both directions. This immediately suggests that MHD turbulence can be quite different from incompressible fluid turbulence, where propagation effects are absent. A simple model, proposed independently by Iroshnikov (1963) and Kraichnan (1965) (referred to as IK phenomenology) is based on the assumption that most of the energy transfer from scales to scales is due to interactions between Alfvenic type of fluctuations. Within the framework of this assumption, Kolmogorov's phenomenology has to be modified to account for the propagation of the "eddies" which limits the time during which they may interact (see for example Dobrowolny *et al*, 1980, Biskamp, 1993). Indeed at scale l there are now two basic time scales, the turn over time $\tau_{NL} \sim l/\delta u_l$ and the Alfven time $\tau_A = l/c_A$ characterizing the time of overlap of two Alfvenic interacting fluctuations propagating in opposite directions. During a time of order t_A the two eddies will exchange only an amplitude of order $\delta u_l \, (\tau_A/\tau_{NL})$; assuming that these interactions occur at random, the number n_c of interactions which is necessary to tranfer an energy $n_c \delta u_l^2 \, (\tau_A/\tau_{NL})^2$ comparable to the initial energy of the eddies is of the order of $n_c \sim (\tau_{NL}/\tau_A)^2$ so that the effective interaction τ_{*l} becomes

$$\tau_{*l} \sim n_c \tau_A \sim \tau_{NL}^2/\tau_A$$

Once again assuming that the energy transfer rate ϵ is constant, one obtains $\delta u_l \sim (\epsilon c_A l)^{1/4}$, corresponding to a power law spectrum in $k^{-3/2}$.

It should be pointed out that this phenomenology is expected to apply only if the external magnetic field is sufficiently strong so that $\tau_A < \tau_{NL}$, the latter time being fixed by the largest scales containing most nof the energy.

3.3 Intermittency

In the phenomenological models described above, it is assumed that the energy transfer rate ϵ is a constant quantity. If one further assumes that the velocity fluctuation δu_l is distributed with a gaussian probability distribution function with a *rms* value $\sim (\epsilon l)^{1/3}$ for neutral fluid turbulence or $(\epsilon c_A l)^{1/4}$ for MHD then its structure functions should behave as

$$S_u^p(l) \sim < \delta u_l^{2p} > \sim l^{\zeta_p} \tag{13}$$

with $\zeta_p = 2p/3$ for neutral fluids or $\zeta_p = 2p/4$ for MHD. This is not what is observed in experiments

or numerical simulations, (see for example Sreenivasan and Antonia, 1997, or Frisch, 1995) where the scaling (13) is indeed observed in the inertial range but with an exponent ζ_p which is not a linear function of p but shows a significant curvature

$$\zeta_p = 2p/3 - \mu_p$$

where the "intermittency' exponents μ_p increase with the order p (compare with the multi affine model of section (2)). This curvature is due to the presence of relatively unfrequent but large bursts of fluctuations which contribute more and more to the structure functions as its order increases. This can be seen in the probability distribution functions of the velocity increment $\delta u_l = \delta u(x+l) - \delta u(x)$ (we are considering only one component of the velocity and only space direction, in order to simplify the notations). These pdf are gaussian for the largest scales, but as the scale diminishes they develop stronger and stronger tails behaving $\exp[-\beta |\delta u_l|^{\nu}]$ for large values of δu_l.

In the intermittent bursts, the velocity signal is even less regular than in the main body of the turbulent fluid and there are many reasons to think that there exists many type of singularities - in the sense of localized regions of very large gradients at the smallest scale of the inertial domain- occupying less and less physical volume as the strength of the singularity increases.

In the standard K41 phenomenology, only the mean value of the energy transfer rate appears in the scaling laws. However one expects that dissipation, especially in a collisionless fluid like the solar wind, will occur in highly localized regions having large gradients - for example by collisionless tearing, etc....i.e.in these "singular regions. Observations and numerical experiments suggest indeed that the stongest "dissipative" events occur in small scale coherent structures (displaying a higher degree of spatial coherence that the surrounding flow, and having longer lifetime), where the transfer rates may have different scaling properties.

Therefore, the deviations from K41 scaling laws seem directly connected to the fact that the transfer rate ϵ is no longer a constant but is random. Many models have been proposed to incorporate this idea into a phenomenological model, and it is outside the scope of this paper to dicuss them (the interested reader is referred to the review by Sreenivasan and Antonia, 1997, or the book by Frisch, 1995). Let us mention only the empirical model proposed by Castaing *et al.* (1990) to fit the observed pdf and the She and Leveque (1994) model which has been rather successful to explain the observed intermittency exponents.

The model developped by Castaing *et al.* (1990) is based upon the idea that if one selects regions having the same value of ϵ, the velocity statistics is gaussian with a variance $\sigma^2(\epsilon)$, but since ϵ is itself a random variable, $\sigma \sim (\epsilon l)^{1/3}$, is also random and fluctuates about $\sigma_0 \sim (\bar{\epsilon} l)^{1/3}$, so that the final pdf is the convolution of a gaussian with the pdf $q(\sigma)$ of σ. This last pdf is chosen to be log normal

$$q(\sigma) = \frac{1}{\lambda\sqrt{2\pi}} \exp\left(-\frac{\ln^2(\sigma/\sigma_0)}{2\lambda^2}\right) d(\ln\frac{\sigma}{\sigma_0})$$

leading to a pdf

$$\Pi(\delta u) = \frac{1}{2\pi\lambda}\int_0^{\infty} \exp\left(\frac{\delta u^2}{2\sigma^2}\right) \exp\left(\frac{\ln^2(\sigma/\sigma_0)}{2\lambda^2}\right) \frac{d\sigma}{\sigma^2}$$

for the velocity fluctuation (at scale l) wich is the superposition of a large number of gaussian distribution with a large extent of width and a weight characterized by only one parameter λ. As we shall see later, this pdf, which represents rather well the experimental results in fluid turbulence and in space plasmas like the the Earth plasma sheet (Angelopoulos *et al.*,1999) is also close to the observed pdf in the solar wind turbulence.

The model by She and Leveque (1994) starts also from the idea that the deviations from K41 scaling laws seem directly connected to the fact that the transfer rate ϵ is no longer a constant but is a random variable, wich, when averaged over a ball of radius l, has a scaling

$$< \epsilon_l^p > \sim l^{\eta_p} \; ; \; < \delta u_l^{2p} > \sim l^{\zeta_p}$$

The basic ideas of the model have some similarities with the previous one, but instead of assuming that the intermittent structures are distributed randomly, the model assumes that there exists a whole hierarchy of structures ranging from that of the "quietly turbulent" flow (labelled 0) with a mean transfer rate ϵ^0 independant of l, to the most active structures (labelled ∞) with a mean transfer rate ϵ^{∞} increasing when the scale l decreases. The K41 scaling uses ϵ^0, while the existence of the other structures account for the deviations to the K41 scaling. Suppose now that the ratio between $< \epsilon_l^{p+1} >$ and $< \epsilon_l^p >$ is due to the structures of order p , characterized by a relative intensity

$$\chi_l^p = \frac{< \epsilon_l^{p+1} >}{< \epsilon_l^p >}$$

which would be = 1 in K41 - the idea being that as p increases more singular structures contribute more and more despite the fact that they occupy a smaller and smaller volume.

Each of these structures results from the balance between the tendency to form highly singular structures and the tendency of the surrounding disorganized flow to disperse them . She and Leveque suggest that this balance imply a dependance of the transfer rate χ^{p+1} on χ^{∞} (tendency to form highly singular structures)

and χ^p(tendency to diserse), which they assume to be of universal form

$$\chi_l^{p+1} \propto (\chi^\infty)^\beta (\chi^p)^{1-\beta}$$

with $\beta < 1$ so that $\chi^p \to \chi^\infty$ as $p \to \infty$. All structures are assumed to have the same lifetime $t_l = (\epsilon_0 l)^{2/3}/\epsilon_0$ but the most active ones are assumed to be able, during that time, to transfer to small scales an energy of the order of that of the largest, energy containing, eddies $\chi^\infty \epsilon^0 = \delta v^2(l_0)/t_l = \epsilon^0 (l/l_0)^{-2/3}$, i.e $\chi^\infty \propto l^{-2/3}$. As a result there is a scaling relation of the form

$$\eta_{p+2} - (1+\beta)\eta_{p+1} + \beta\eta_p + \frac{2}{3}(1-\beta) = 0$$

which has the solution

$$\eta_p = -\frac{2}{3}p + 2\left(1 - \left(\frac{2}{3}\right)^p\right)$$

leading to

$$\zeta_p = \frac{p}{9} + 2\left(1 - \left(\frac{2}{3}\right)^p\right)$$

for the scaling laws for the velocity structure functions. An extension of this model to the MHD case was proposed by Politano and Pouquet (1995), in the framework of the IK phenomenology.

Coming back to the Haar wavelet transform this discussion suggests to use some conditionning of the wavelet spectra and structure functions to separate the "quietly turbulent" flow , characterized by a mean transfer rate ϵ^0 independant of l, from the other, more active structures. Conditional sampling techniques have been widely used to extract coherent events from data records; wavelets are particularly well suited for this purpose, because they allow This has been done for example by Katul *et al.* (1994), in the analysis of the atmospheric surface layer turbulence and by Veltri and Mangeney (1999). The idea is to separate, at a given scale m, the wavelet coefficients into two classes according to their amplitude, those which are below a certain threshold a_*^m, $|a_y(i,m)| < a_*^m$, what happens at time indices i belonging to some subset $\Sigma = [i_1, i_2, ...]$ of the interval $[1, N]$ which characterizes the "quietly turbulent" flow and those with $|a_y(i,m)| > a_*^m$ which characterizes the intermittent regions.

The conditionned structure functions are defined by equations similar to (5), except that the sum representing the average value is calculated only points whose index belong to Σ. To choose a meaningful threshold, one may think to use the empirically determined pdf of $a_y(i,m)$, but as we shall see later on, their shape does not contain any feature which would justify a particular choice. Thus one is left with the lowest order moment $< |a_y(i,m)|^2 >$ the average being taken over all points and the choice is $(a_*^m)^2 = F < |a_y(i,m)|^2 >$,

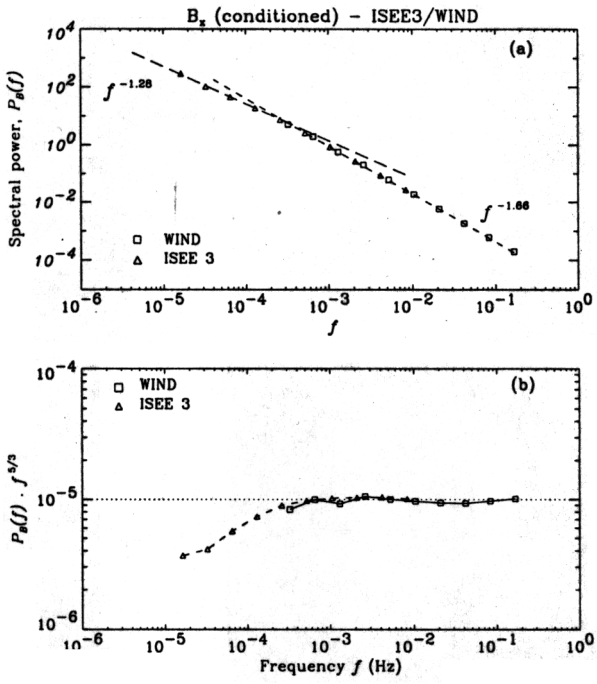

Figure 5: Conditionned power spectra for the ISEE3 (triangles) and Wind (squares) x_{GSE} component of the magnetic field

the conditionning criteria being chosen so that not too many points are excluded by the conditionning. Usually $F \sim 10$, corresponding to the elimination of a few percent of the points, and results practically independant *of* the precise value of F.

4 The WIND observations

We have already given in the introduction some characteristics of the data which we shall use here, the magnetic field from the MFI experiment and the plasma data from the 3D-Palsma experiment, all sampled continuously with a 3 sec resolution. For most of the study described below we have used $N = 2^{19}$ data points, what allows to determine sufficiently accurately structure functions of order up to $p = 9$.

It should be noted that the low frequency spectrum of the magnetic field shown in figure 1 are actually conditionned wavelet spectra, with $F = 10$.This explains its smoothness, which allow an easy and accurate determination of the spectral slope. In particular, one can specify the extent of the inertial domain, where the spectrum has a clear power law shape.

This is illustrated in Figure 5 which presents in its upper panel a comparison between the Wind data -with a resolution of 3 sec and the ISEE data with a resolution of 1min for the x_{GSE} -component of the magnetic field. Note that the two sets of data almost coincide-altough they were taken at distant times, of the order

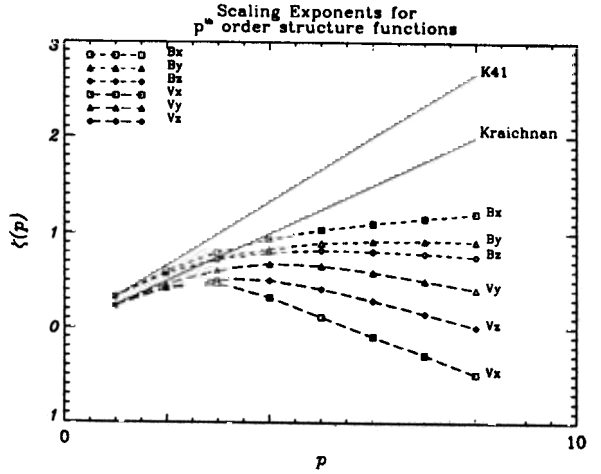

Figure 6: Scaling exponents ζ_p, equation (13), for the structure functions of $B_x, B_y, B_z, v_x, v_y, v_z$

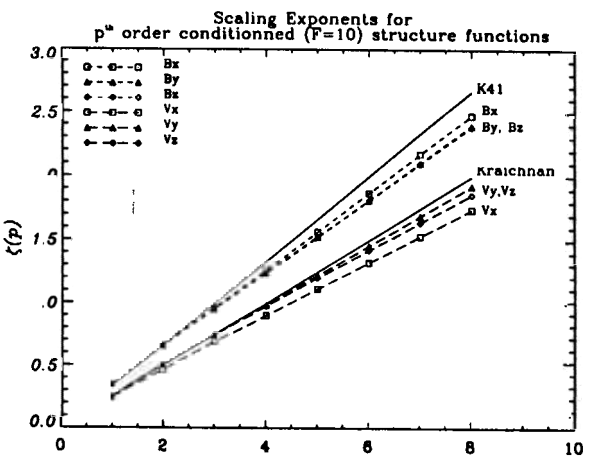

Figure 7: Same as figure 6, but after conditionning

of a decade!

There appears to be a break in the spectral slope around a frequency $f \sim 10^{-4}Hz$ above which the spectrum becomes a K41 power law. This is confirmed by the lower panel of Figure 5 which displays the two spectra multiplied by $f^{5/3}$. One sees immediately that the compensated spectrum is almost flat in the domain $10^{-4} - 10^{-1}$Hzi. Therefore the inertial range of the Alfvenic turbulence in the solar wind appears to extend from frequencies of order $f \sim 10^{-4}Hz$ up to the cyclotron frequency (Leamon *et al.*, 1998).

The structure functions

$$< \delta\psi_\tau^p >=< |\psi(t+\tau) - \psi(t)|^p >$$

have been calculated up to order $p = 8$ for the quantities $\Psi = \{B_x, B_y, B_z, v_x, v_y, v_z\}$. In figure 6, upper panel, we have plotted the structure functions for B_x and v_x as a function of the time scales $\tau_m = 2^m \Delta t$ to illustrate their general behavior. When nothing particular is done, their shape is consistent with a power law behavior $< \delta\psi_\tau^p > \sim \tau^{\zeta_p}$ only for the lowest value of p, especially for the radial velocity. One can still determine the exponents ζ_p by fitting the structure functions with power laws, although this determination becomes less and less accurate as p increases. The result is shown in figure 6 which displays ζ_p versus p together with the two linear laws expected with the K41 or IK phenomenologies. As shown by Burlaga (1991), Marsch and Liu (1993), Veltri and Mangeney (1999) there is a strong deviation from gaussianity, even stronger than in hydrdynamic turbulence.

On the other hand after conditioning with a moderate threshold, $F = 5$, which eliminates less than 4% of the data, the same structure functions exhibit a nice power law behaviour, see equation (13) up to $p = 8$ allowing a precise determination of ζ_p, which when plotted against p (figure ??) exhibit a linear dependance

$$\zeta_p \simeq \gamma p$$

($\gamma = 0.306$) suggesting that one has effectively eliminated the most active, intermittent structures. It should however be noted that the slopes are different for different quantities. Surprinsingly the velocity components cluster around the K41 line, while the magnetic field components cluster around the IK line.

Another possible description of the same information is through the probability distribution functions of the fluctuations, here the wavelet coefficients. Several authors (Burlaga, 1993, Feynman and Ruzmaikin, 1994, Marsch and Tu, 1997) have shown that these pdf's are essentially gaussian for time scales longer than a few hours, but show strong deviations from gaussiannity at smaller scales.

Figure 8 displays the six probability distribution functions (normalized histograms) of the components of Ψ, for all accessible scales, but after a rescaling of the abcissa

$$\delta\tilde{\psi}_m = 2^{-(m-1)(\gamma+\frac{1}{2})}\delta\psi_m$$

and the corresponding rescaling of the probability distribution function. There is a very trong similarty to what was observed in the multiaffine exemple of section (2) and this figure demonstrates in particular that here also, there is a self similar structure over the inertial range.

What is the nature of the "intermittent events"? Let us look at the "singular" points which have been left when working on the conditioned structure functions. The technique used here is to consider an interval of data around the local maximum of the amplitude of the wavelet coefficient at the smallest case, to perform a minimum variance analysis of the magnetic field during this interval: if the mimimum eigenvalue is sufficiently small with respect to the wo others, then there

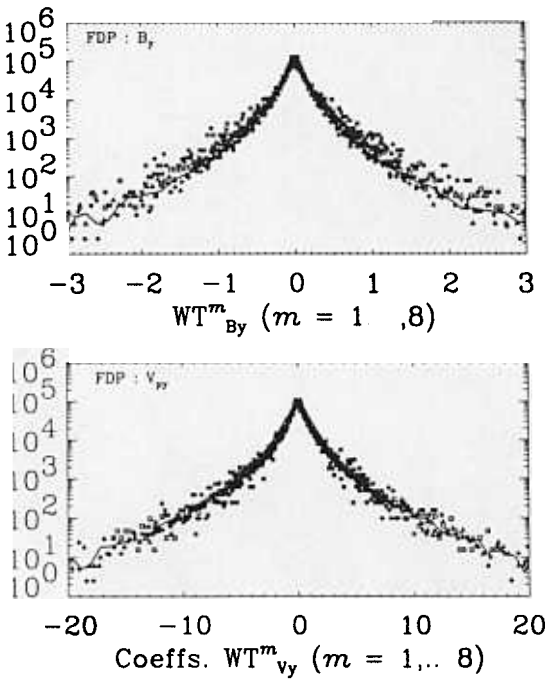

Figure 8: Probability density distributions for the scales $m = 1 - 8$ of the wavelet coefficients of v_y and B_y

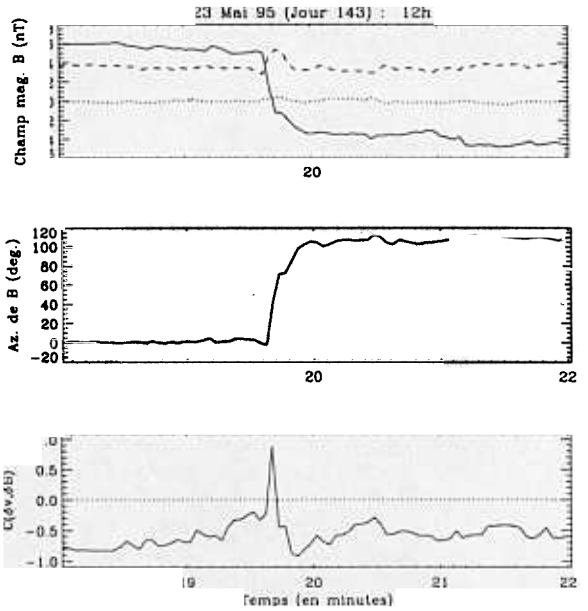

Figure 9: A current layer; the three components of the magnetic field in the minimum variance reference frame are shown in the upper panel; the middle panel displays the rotation angle of the magnetic field in the plane perpendicular to the direction of minimum variance and the lower panel shows the evolution of the degree of alignment between the velocity and magnetic perturbations

is good reasons to think that the "singularity" has at least locally a sheetlike geometry.

We shall not present here an exhaustive description of all structures which are detected in this way. Let us briefly describe one of the most common, current sheet type , an example from day 143 of 1995 being given in figure 9.

The upper panel displays the three components of the magnetic field in the principal axis of the minimum variance analysis while the lower panel displays the evolution of the ratio $\delta\mathbf{v}\cdot\delta\mathbf{B}/(\delta v_{rms}\delta B_{rms})$ measuring the degree of alignment of the perturbations in the two fields (the average magnetic field and velocity for the period analyzed have been substracted, while the resulting perturbations $\delta\mathbf{v}$ and $\delta\mathbf{B}$ have been normalized to their total *rms* value during the same interval). In this case there are two small eigenvalues and it is hard to determine wether it is a one or two dimensional structure.

Besides this current layers, the "singularities" can take the form of shock waves, magnetic holes, soliton like Alfvenic perturbations, which will be described in detail in future papers.

5 References

Angelopoulos, V., T. Mukai and S. Kokobun, 1999, Phys. Plasmas, **6**, 4161

Benzi, R., L. Biferale, A. Crisanti, G. Paladin, M. Vergassola, and A. Vulpiani, 1993, Physica D, **65**, 352

Biskamp, D., 1993, *Nonlinear Magnetohydrodynamics*, Cambridge University Press, Cambridge, UK

Bougeret, J.-L., M.L. Kaiser, P.J. Kellogg, R. Manning, K. Goetz, S.J. Monson, N. Monge, L. Friel, C.A. Meetre, C. Perche, L. Sitruk, S. Hoang, Space Sci. Rev., **71**, 231

Burlaga, L.F., 1991, J. Geophys. Res., **96**, 5847

Castaing, B., Y. Gagne and E.J. Hopfinger, 1990, PhysicaD, **46**, 177

Dobrowolny, M., A. Mangeney and P.L. Veltri, 1980, Phys. Rev. Lett., **45**, 144

Doob, J.L.,1953, *Stochastic processes*, Wiley, New York

Elsässer, W., M., 1950, Phys.Rev., **79**, 183

Elsässer, W., M., 1956, Rev. Mod. Phys., **18**,135

Feynman, J. and A. Ruzmaikin, 1994, J. Geophys. Res., **99**, 17645

Frisch, U., 1995, *Turbulence*, Cambridge University Press, Cambridge, UK

Goldstein, M.L. and D.A. Roberts, 1995, Ann. Rev. Fluid Mech., **33**, 283

Grappin, R., M. Velli and A. Mangeney, 1991, Ann. Geophysicae, **9**, 416

Horbury, T.S., 1999, in *Proceedings of the International Conference on Plasma Turbulence and Energetic Particles in Astrophysics* , M. Ostrowski and R. Shlickeiser (Eds.), Cracow, Poland, p. 115

Iroshnikov, P., S., 1963, Astron. Zh., **40**,742

Katul, G.G., J.D. Albertson, C.R. Chu and M.B. Parlange, 1994, in *Wavelet in Geophysics*, E. Foufoula and P. Kumar (Eds.), Academic Press, San Diego, USA

Kolmogorov, A., N., 1941, Doklady Acad. Sci. U.S.S.R., **31**, 6

Kraichnan, R., H., 1965, Phys. Fluids, **8**, 1385

Leamon, R.J., C.W. Smith, N.F. Ness, W.H. Matthaeus, and H.K. Wong, 1998a, J.Geophys. Res., **103A**, 4775

Lepping, R.P., M.H. Acűna, L.F. Burlaga, W.M. Farrell, J.A. Slavin, K.H. Schatten, F. Mariani, N.F. Ness, F.M. Neubauer, Y.C. Whang, J.B. Byrnes, R.S. Kennon, P.V. Panetta, J. Scheifele, and E.M. Worley, 1995, Space Sci. Rev., **71**, 207

Lin, R.P., K.A. Anderson, S. Ashford, C. Carlson, D. Curtis, R. Ergun, D. Larson, J. McFadden, M. McCarthy, G.K. Parks, H. Rème, J.-M. Bosqued, J. Coutelier, F. Cotin, C. d'Uston, K.-P. Wenzel, T.R. Sanderson,J. Henrion, J.C. Ronnet, G. Paschmann, 1995, Space Sci. Rev., **71**, 125

Mangeney A., R. Grappin, M. Velli, 1991, in *Proc. MHD Symposium, Advances in Solar System Magnetohydrodynamics*, E.R. Priest and A.W. Hood (Eds.), St Andrews,Scotland, p. 344

Marsh,E., Tu C.Y., 1997, Nonlinear Processes in Geophysics, **4**, 101

Marsh, E. and Liu S., 1993, Ann. Geophysicae,textbf11, 227 She Z.S., Lévêque E., 1994, Phys.

Rev. Lett., **72**, 336

Politano, H., and A. Pouquet, 1995, Phys. Rev. E,**52**, 636 Sreenivasan, K.R. and R.A. Antonia, 1997, Ann.

Rev. Fluid Mech., **29** , 435

Tu, C.Y. and E. Marsch, 1995, Space Sci. Rev., **73**, 1

Veltri, P.L., and A. Mangeney,1999, in *Solar Wind 9*, S.R. Habbal, R. Hesser, J.V.Hollweg and P.A. Isenberg (Eds.), American Institute of Physics, New York, p. 543